Controlling transition matrix elements and relaxation in a two-electron double quantum dot

Carlos F. Destefani,* Chris McDonald,† Suren Sukiasyan, and Thomas Brabec
Department of Physics and Center for Photonics Research, University of Ottawa, Ottawa, Ontario, Canada K1N6N5
(Received 13 August 2008; revised manuscript received 2 April 2009; published 27 April 2009)

We demonstrate theoretically that transition matrix elements between ground and first-excited singlet states of a two-dimensional two-electron lateral double quantum dot can be controlled and changed by orders of magnitude by varying the interdot barrier. As a result, decay arising from system-environment coupling can be controlled. A potential ramp is identified by which the system is nonadiabatically inverted and then frozen by insulating it against environmental decay.

DOI: 10.1103/PhysRevB.79.155322 PACS number(s): 73.21.La, 03.67.Pp, 42.50.Lc, 63.20.kd

I. INTRODUCTION

Our ability to manipulate matter on a microscopic level rests on creating transitions between eigenstates of a system by introducing a perturbation. The resulting quantum dynamics of the system and between the system and the environment is governed by transition matrix elements (TMEs). For a given perturbation, they are inherent properties of the microscopic system under investigation and can only be changed when the confining potential is changed. Whereas this is very difficult in atomic and molecular physics, tools exist in semiconductor physics by which the confining potential can be changed.[1,2]

Our theoretical analysis shows that a two-dimensional (2D) two-electron lateral double quantum dot[3–6] (DQD) is particularly suitable for this purpose. The TME between ground and first-excited state, with regard to a general perturbation, can be controlled over orders of magnitude by exploiting the different charge correlation properties of these two states. In the limit of an infinitely high interdot barrier, the ground state of a highly biased DQD has a (0,2) charge configuration, with two electrons in one dot. The first-excited state is in a (1,1) configuration with one electron in each dot. Due to the different charge distribution characters, the wave functions of these two states have no overlap; therefore, TMEs between them are zero. As a result, environmentally induced relaxation is turned off and the population of the two-level system is frozen. This is explicitly demonstrated here for coupling to phonon and photon baths. When the interdot barrier is ramped down, the (0,2) and (1,1) charge configurations start to mix and the TMEs are switched on so that the two-level system can be manipulated.

We identify an electric pulse that inverts and freezes the population of the two-level system by modifying the bias and the barrier between the two quantum dots. The capacity to control decay over orders of magnitude is mostly of fundamental interest. Potential applications are discussed at the end of the paper.

The scope of our paper is as follows. Section II shows the time-dependent Schrödinger equation, Hamiltonian of our system, and its spectrum. Section III states the multiconfiguration time-dependent Hartree-Fock (MCTDHF) formalism, which is used to handle the electron dynamics in our problem; the wave function in MCTDHF is expanded as a sum over many-electron configurations, where both the expansion coefficients and the single-particle basis set are time dependent.[7–10] Section IV discusses the control and freezing of transition matrix elements by dynamical manipulation of our two-level singlet subspace. In Sec. V two potential applications of our study are discussed.

II. HAMILTONIAN AND TWO-ELECTRON SPECTRUM

The two-electron dynamics in the DQD is described by the Schrödinger equation in effective atomic units

$$i\frac{\partial}{\partial t}\Psi = H(\mathbf{r}_1,\mathbf{r}_2,t)\Psi = \left[\sum_{i=1}^{2} H_1(\mathbf{r}_i,t) + H_2(\mathbf{r}_1,\mathbf{r}_2)\right]\Psi, \quad (1)$$

where $\mathbf{r}=(x,y)$ and the in-plane wave function is $\Psi = \Psi(\mathbf{r}_1,\mathbf{r}_2,t)\otimes|S\rangle$. The spin singlet state $|S\rangle = |\uparrow(1)\downarrow(2) - \downarrow(1)\uparrow(2)\rangle$ is conserved throughout our analysis. The one-electron Hamiltonian is $H_1 = T + V(\mathbf{r},t)$, with $T=-\nabla^2/2$ as the kinetic-energy operator and $V(\mathbf{r},t)$ as the potential of the DQD. Further, the two-electron Hamiltonian is $H_2 = 1/\sqrt{(\mathbf{r}_2-\mathbf{r}_1)^2+a^2}$, where the parameter a arises from the finite thickness of the 2D DQD. For the calculation of phonon decay below, three-dimensional (3D) bulk properties are required. For that we consider the z direction to be confined by a quantum well of size a, centered at $z=0$; the confinement is strong enough that only the lowest vertical subband is populated. The resulting 3D wave function is $\Psi(\mathbf{r}_1,\mathbf{r}_2,t) \otimes Z(z_1,z_2)$, with $Z(z_1,z_2)=\phi(z_1)\otimes\phi(z_2)$ and $\phi(z) = \sqrt{2/a}\cos(\pi z/a)$.

In our analysis, we consider a GaAs DQD with an effective mass $m=0.067$ and a dielectric constant $\nu=12.4$. The effective atomic units used throughout the paper are then size in effective Bohr radius $R^*=9.80$ nm, energy in effective Hartree energy $E^*=11.85$ meV, and time in effective natural time $T^*\equiv\hbar/E^*=55.55$ fs.

The lateral DQD potential $V(\mathbf{r},t)=V_l(\mathbf{r},t)+V_b(\mathbf{r},t) + V_r(\mathbf{r},t)$ consists of the left dot, right dot, and central barrier contributions $V_i(\mathbf{r},t)=W_i(t)U_i(\mathbf{r})(i=l,r,b)$ with Gaussian shape $U_i(\mathbf{r})=\exp[-(\mathbf{r}-\mathbf{d}_i)^2/\Delta_i^2]$, width Δ_i, and depth $W_i(t)$. The left dot, right dot, and barrier are centered at $\mathbf{d}_l = (-d,0)$, $\mathbf{d}_r=(+d,0)$, and $\mathbf{d}_b=(0,0)$, respectively, with $2d$ as the distance among the dots. In our analysis, $W_r(t)=W + \epsilon(t)$ and $W_b(t)$ are biased with time, while $W_l(t)=W$ is held constant. The potential detuning between the two dots is $\epsilon(t)=W_r(t)-W$. Notice that the bias is applied to the right dot

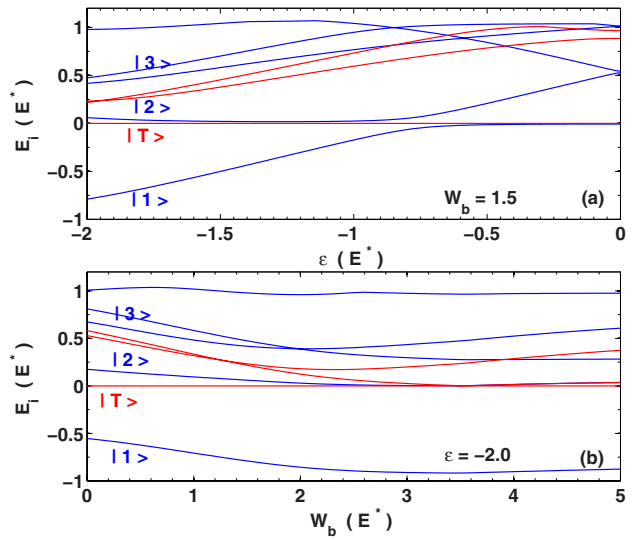

FIG. 1. (Color online) DQD two-electron energy spectrum E_i as a function of the detuning ϵ between the dots [$W_b=1.5$, panel (a)] and as a function of the interdot barrier W_b [$\epsilon=-2$, panel (b)]. The spectrum (singlets in blue and triplets in red) is shown with reference to the lowest triplet $|T\rangle$. Only the lowest five (three) singlets (triplets) are shown with the lowest three singlets explicitly labeled.

and that $\epsilon=0(\epsilon<0)$ stands for a symmetric (asymmetric) potential profile, with $\epsilon=-2$ for the most asymmetric profile we use; when it is the interdot barrier that is varied, W_b ranges from 0 (highly coupled DQD) to 5 (highly decoupled DQD limit). The DQD parameters $\Delta_l=\Delta_r=2.5$, $\Delta_b=1.5$, $W=-5$, $d=2$, and $a=0.5$ remain fixed throughout the paper.

The size of our DQD is smaller than the size used in GaAs DQD experiments.[3–6] This choice is driven by numerical convenience. Larger dots have a more closely spaced spectrum and require a much finer grid resolution which is difficult to handle numerically. However, we would like to stress that the results derived in the following are general and do neither depend on the size of our DQD nor the choice of Gaussian[11,12] potentials $V(\mathbf{r},t)$. Calculations with somewhat larger dots and different potentials, e.g., a harmonic potential,[13,14] have given similar results.

The parameters used here were chosen to achieve a two-electron spectrum, see Fig. 1, qualitatively similar to the experimental spectra of such systems.[3,4] Panel (a) shows the spectrum as a function of ϵ at fixed $W_b=1.5$, while panel (b) does the same but as a function of W_b at fixed $\epsilon=-2$; the energy levels are plotted with reference to the lowest triplet $|T\rangle$; only the lowest five (three) singlets (triplets) are shown. The two-electron energies E_i and eigenstates $|i\rangle\equiv|\Psi_i\rangle$ are obtained by diagonalizing the configuration interaction matrix of Hamiltonian H in Eq. (1) with respect to the eigenstates of H_1 for each related set of DQD parameters; in Fig. 1 the lowest three singlets, $|1\rangle$, $|2\rangle$, and $|3\rangle$ are explicitly labeled. A basis of 50 spatially distinct one-electron orbitals ($n=100$ spin orbitals), yielding 4950 two-electron configurations, is sufficient to converge the first few singlet and triplet states.

In the following the properties of the lateral DQD used in our investigation are further specified: (i) the distance between the dots is $2d=4\approx40$ nm and $a=0.5\approx5$ nm. If we define the lateral/vertical ratio as $2d/a$, it amounts to 8 in our system. (ii) The single-electron lowest energy spacing ω_0 of the isolated (e.g., right) dot can be inferred from $\sqrt{2|W_r|/\Delta_r}$, ranging from ≈14.99 meV at $W_r=-5$ to ≈17.73 meV at $W_r=-7$; further, the one-electron bonding and antibonding lowest-energy spacings ω_{SAS} of the coupled double dot is a function of both ϵ and W_b; at, e.g., $W_b=1.5$, such splitting is ≈14.6 meV at $\epsilon=-2$ and ≈0.89 meV at $\epsilon=0$. (iii) The transition energies between the two-electron states in Fig. 1(a), which are relevant for our analysis, are for $\epsilon=0$, $\delta_{|1\rangle-|T\rangle}=0.0070\approx0.083$ meV, $\delta_{|2\rangle-|T\rangle}=0.5269\approx6.244$ meV, and $\delta_{|2\rangle-|3\rangle}=0.0167\approx0.198$ meV, and for $\epsilon=-2\approx23.7$ meV, $\delta_{|1\rangle-|T\rangle}=0.7852\approx9.305$ meV, $\delta_{|2\rangle-|T\rangle}=0.0582\approx0.690$ meV, and $\delta_{|2\rangle-|3\rangle}=0.3575\approx4.236$ meV. As the barrier is increased in Fig. 1(b) for $\epsilon=-2$, among other features, the singlet $|3\rangle$ crosses with the next-excited singlet; in what follows, the label $|3\rangle$ always refers to the third lowest singlet in energy at the related DQD configuration.

III. MCTDHF AND TWO-ELECTRON DYNAMICS

Equation (1) is solved by the MCTDHF approach,[7–10] which relies on the ansatz

$$\Psi(\mathbf{r}_1,\mathbf{r}_2,t)=\sum_{j_1\neq j_2=1}^{n}A_{j_1j_2}(t)\phi_{j_1}(\mathbf{r}_1,t)\phi_{j_2}(\mathbf{r}_2,t)s_{j_1}(1)s_{j_2}(2), \tag{2}$$

confined here to two electrons for the sake of simplicity. The n single-particle basis functions are characterized by a spin $s_j=\uparrow,\downarrow$ and by an orbital part ϕ_j. We use restricted MCTDHF with $n/2$ different orbital basis functions; the resulting number of configurations is $\binom{n}{2}$. The antisymmetry of the wave function $\Psi(\mathbf{r}_1,\mathbf{r}_2,t)$ is ensured by imposing the constraint $A_{j_1j_2}=-A_{j_2j_1}$ on the expansion coefficients. Both $A_{j_1j_2}(t)$ and $\phi_j(\mathbf{r},t)$ are time dependent and are determined by the Dirac-Frenkel variational principle

$$\langle\delta\Psi(t)|i\frac{\partial}{\partial t}\Psi(t)-H(t)|\Psi(t)\rangle=0. \tag{3}$$

Performing the variation with regard to Eq. (2) yields a set of time-dependent nonlinear coupled integrodifferential equations for $A_{j_1j_2}(t)$ and $\phi_j(\mathbf{r},t)$,

$$i\frac{\partial}{\partial t}A_{j_1j_2}(t)=\sum_{l_1\neq l_2=1}^{n}H_{j_1j_2l_1l_2}(t)A_{l_1l_2}(t), \tag{4}$$

$$i\frac{\partial}{\partial t}\phi_j(\mathbf{r},t)=(1-P(\mathbf{r},t))\sum_{k,l=1}^{n}R_{jlk}(\mathbf{r},t)\phi_k(\mathbf{r},t), \tag{5}$$

where $R_{jlk}(\mathbf{r},t)=\rho_{jl}^{-1}(t)\langle H\rangle_{lk}(\mathbf{r},t)$, with $\rho_{jl}(t)=\Sigma_{i=1}^{n}A_{ji}^{\star}(t)A_{li}(t)$ as the density matrix. Further, the projector is $P(\mathbf{r},t)=\Sigma_{i=1}^{n}|\phi_i(\mathbf{r},t)\rangle\langle\phi_i(\mathbf{r},t)|$ and the mean field is given by

$$\langle H\rangle_{lk}(\mathbf{r},t)=\sum_{i=1}^{n}\langle A_{li}(t)\phi_i(\mathbf{r}_2,t)|H(t)|A_{ki}(t)\phi_i(\mathbf{r}_2,t)\rangle, \tag{6}$$

while the two-electron matrix elements are given by

$$H_{j_1 j_2 l_1 l_2}(t) = \langle \phi_{j_1}(\mathbf{r}_1,t)\phi_{j_2}(\mathbf{r}_2,t)|H(t)|\phi_{l_1}(\mathbf{r}_1,t)\phi_{l_2}(\mathbf{r}_2,t)\rangle. \tag{7}$$

To clarify how the MCTDHF wave function is constructed, we detail the ansatz in Eq. (2) for the simplest case of $n=4$ spin orbitals, that is, $\{\phi_j\} \equiv \{\phi_1, \phi_2, \phi_3, \phi_4\}$ with $\{s_j\} \equiv \{\uparrow_1, \uparrow_2, \downarrow_3, \downarrow_4\}$. In a restricted basis set, two up and two down spin orbitals are present, with only $n/2=2$ distinct spatial parts, that is, $\phi_3=\phi_1(\downarrow_3=\downarrow_1)$ and $\phi_4=\phi_2(\downarrow_4=\downarrow_2)$. Altogether, the restricted basis set becomes $\{\phi_j s_j\} \equiv \{\phi_1\uparrow, \phi_2\uparrow, \phi_1\downarrow, \phi_2\downarrow\}$. By using the constraint $A_{j_1 j_2}=-A_{j_2 j_1}$, Eq. (2) can then be expressed as

$$\begin{aligned}
\Psi(\mathbf{r}_1,\mathbf{r}_2,t) = {} & A_{12}(t)[\phi_1(\mathbf{r}_1,t)\phi_2(\mathbf{r}_2,t) - \phi_2(\mathbf{r}_1,t)\phi_1(\mathbf{r}_2,t)]\uparrow(1)\uparrow(2) \\
& + A_{13}(t)\phi_1(\mathbf{r}_1,t)\phi_1(\mathbf{r}_2,t)[\uparrow(1)\downarrow(2) - \downarrow(1)\uparrow(2)] \\
& + A_{14}(t)[\phi_1(\mathbf{r}_1,t)\phi_2(\mathbf{r}_2,t)\uparrow(1)\downarrow(2) - \phi_2(\mathbf{r}_1,t)\phi_1(\mathbf{r}_2,t)\downarrow(1)\uparrow(2)] \\
& + A_{23}(t)[\phi_2(\mathbf{r}_1,t)\phi_1(\mathbf{r}_2,t)\uparrow(1)\downarrow(2) - \phi_1(\mathbf{r}_1,t)\phi_2(\mathbf{r}_2,t)\downarrow(1)\uparrow(2)] \\
& + A_{24}(t)\phi_2(\mathbf{r}_1,t)\phi_2(\mathbf{r}_2,t)[\uparrow(1)\downarrow(2) - \downarrow(1)\uparrow(2)] \\
& + A_{34}(t)[\phi_1(\mathbf{r}_1,t)\phi_2(\mathbf{r}_2,t) - \phi_2(\mathbf{r}_1,t)\phi_1(\mathbf{r}_2,t)]\downarrow(1)\downarrow(2),
\end{aligned} \tag{8}$$

where $\binom{n}{2}=6$ distinct coefficients (configurations) are present. The first and sixth lines in Eq. (8) are triplets with $S_z=1$ and $S_z=-1$, respectively, while the second and fifth lines are singlets with doubly occupied orbitals. For Eq. (8) to be fully antisymmetric, the third and fourth coefficients have to be interdependent; when $A_{14}=\pm A_{23}$, the third and fourth lines become $A_{14}(t)[\phi_1(\mathbf{r}_1,t)\phi_2(\mathbf{r}_2,t) \pm \phi_2(\mathbf{r}_1,t)\phi_1(\mathbf{r}_2,t)][\uparrow(1)\downarrow(2) \mp \downarrow(1)\uparrow(2)]$, in which the upper (lower) sign refers to a singlet (triplet with $S_z=0$).

The singlet ground state at $t=0$ is found via imaginary time propagation. The only restriction imposed on the MCTDHF coefficients is that $A_{j_1 j_2}=-A_{j_2 j_1}$; the interdependence of some coefficients, like between A_{14} and A_{23} in the simple example above, building up the fully antisymmetric ground-state wave function comes out naturally in the imaginary propagation of Eqs. (4) and (5). After a given time of imaginary propagation, only the ground state survives, yielding the converged set of orbitals and coefficients to be used as the initial state at $t=0$ in the real propagation of Eqs. (4) and (5). The real propagation yields the many-particle wave function in Eq. (2) at any time instant. Notice that the time evolution does not alter the spin character of the initial state since Hamiltonian is spin independent; that is, once the propagation starts from a given singlet, the system will always remain in a singlet. Finally, notice that the time-dependent configuration-interaction method is a special case of MCTDHF which occurs when an infinite basis set is used, that is, $P=1$ in Eq. (5), so that the orbitals become time independent and only the coefficients are propagated.

IV. CONTROL OF TRANSITION MATRIX ELEMENT

Lateral DQDs are a promising medium for quantum computation. In contrast to spin qubit implementations,[3,4] where the subspace under study is formed by the lowest singlet $|1\rangle$ and triplet $|T\rangle$ states, our analysis focuses on the subspace formed by the two lowest singlets, $|1\rangle$ and $|2\rangle$.

Figure 1(a) shows that it is difficult to address such a two-level singlet subspace at $\epsilon=0$ because the singlet $|3\rangle$ is too close. For that reason, we focus on the asymmetric limit of $\epsilon=-2$. Figure 1(b) shows how the transition energies at $\epsilon=-2$ evolve, when the interdot barrier W_b is increased from 0 to 5.0 (59.25 meV).

The basic concept underlying the control of TMEs between ground ($|1\rangle$) and first-excited ($|2\rangle$) singlets of a two-electron DQD can be understood from Figs. 2 and 3, both at $\epsilon=-2$. In Fig. 2, the probability of the possible charge configurations, (N_l,N_r), of the lowest three singlets is plotted in panels (a)–(c) as a function of W_b; Fig. 3 shows the correlated (x_1,x_2) electron distribution $|\Psi_i|^2$, which indicates the charge character of the related state for the same lowest three singlets (from left to right) at a low barrier $W_b=1.5$ (upper panel) and at a high barrier $W_b=5$ (lower panel). The charge configuration probability is determined by first integrating $|\Psi_i|^2$ over the whole y_1,y_2 simulation box; this yields the two-electron probability as a function of x_1 and x_2. From these two-dimensional probabilities (N_l,N_r) is determined by integrating over the respective x_1,x_2 integration areas depicted in Fig. 2(d).

Whereas for a low interdot barrier the eigenstates contain a mix of different charge configurations for increasing W_b the eigenstates go over into pure charge configurations as seen in Fig. 2; in the limit of an infinitely high W_b, all eigenstates take a pure charge configuration. Figure 3 clearly shows how the lowest three singlet states acquire pure (0,2), (1,1), and (0,2) charge characters, respectively, as one moves from low to high interdot barrier; the very small (0,2) component remaining in $|2\rangle$ disappears at a higher W_b. In such highly asymmetric DQD, singlets with (2,0) character can only occur at very high excitation energies.

As two eigenstates with different two-electron charge configurations are in disjoint parts of the simulation volume, their overlap, and hence their product approach zero, e.g.,

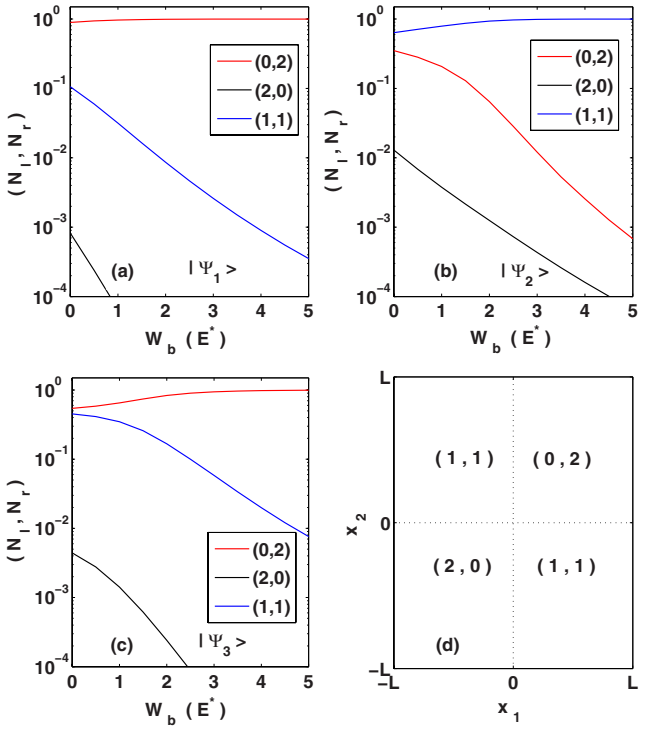

FIG. 2. (Color online) [(a)–(c)] Probability of two-electron charge configurations, (N_l,N_r), for the lowest three singlets as a function of the interdot barrier W_b. (d) x_1,x_2 integration areas for the various charge configurations; a square simulation box is employed with $L=10$ and $N=64$ points per dimension. In panels (a) and (c) [panel (b)] the dominant charge character is (0,2) [(1,1)], while (2,0) has always the smallest contribution for these three singlets.

$\Psi_1^*(\mathbf{r}_1,\mathbf{r}_2)\Psi_2(\mathbf{r}_1,\mathbf{r}_2)\approx 0$ for all $\mathbf{r}_1$ and $\mathbf{r}_2$. Therefore, the TME with respect to a general one- or two-electron operator $\hat{\mathbf{O}}$ vanishes, $\hat{\mathbf{O}}_{12}=\langle 1|\hat{\mathbf{O}}|2\rangle\approx 0$. In this limit, transitions between these two states are disabled, and the first-excited singlet state is preserved against environmentally induced decay. Note that because all eigenstates are in a pure charge configuration at high W_b, all transition channels between $|1\rangle$ and $|2\rangle$ are suppressed, including higher-order transitions taking place via intermediate excited states. When W_b is decreased, the (0,2) and (1,1) configurations in $|1\rangle$ and $|2\rangle$ start to mix, and the TME $\hat{\mathbf{O}}_{12}$ is switched on. It is worth mentioning that such vanishing of the TME is of fundamental nature in two- or few-electron DQDs, and it is independent of the specific choice of the single-particle confining potential.

A. Freezing of the two-level singlet subspace

Freezing the population in the first-excited state by switching off environmentally induced decay is demonstrated in Fig. 4, where phonon ($\tau_{\text{phonon}}=1/\Gamma$) and spontaneous photon ($\tau_{\text{photon}}=1/\gamma$) emission times from $|2\rangle$ to $|1\rangle$ are plotted as a function of W_b for the highly biased DQD with $\epsilon=-2$. Both photon and phonon interactions take place in the THz frequency regime. For the phonon emission rates, we take into account deformation acoustic phonons[15,16] in polar zinc-blende structures; the influence of piezoelectric acoustic phonons and higher energetic optical phonons were found to be 3 orders of magnitude smaller, and therewith negligible in our system. Further, we assume that no excitons and holes exist so that decay by optical-interband transitions can be excluded.

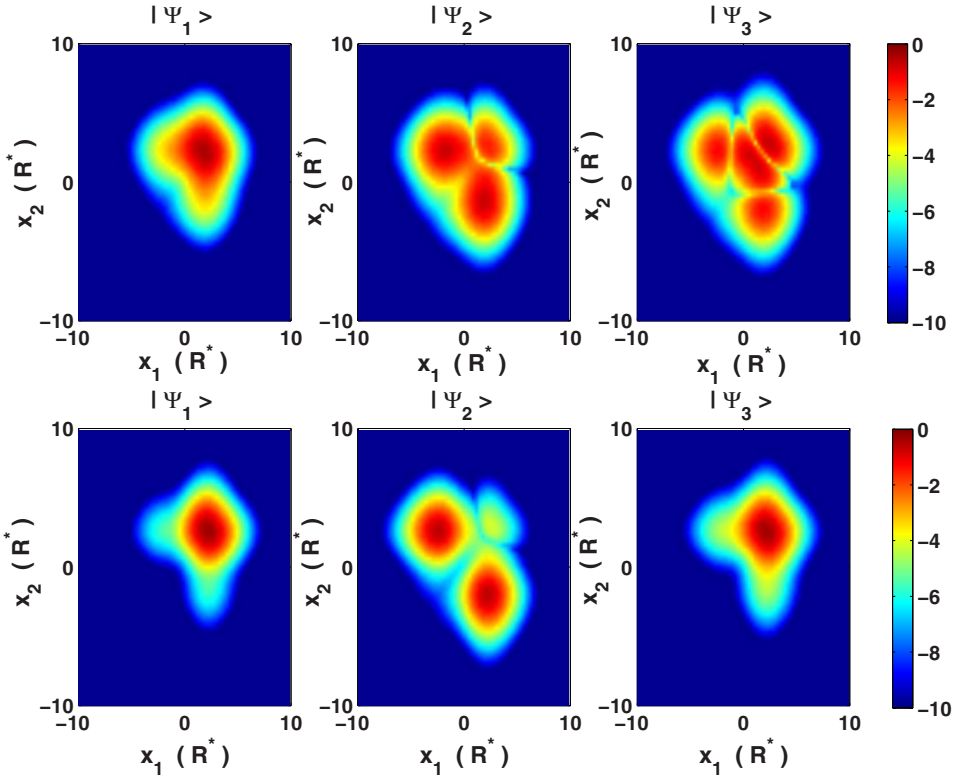

FIG. 3. (Color online) Two-electron eigenstates $|1\rangle$, $|2\rangle$, and $|3\rangle$ (from left to right) at $\epsilon=-2$; probability $|\Psi_i|^2$, integrated over y_1,y_2, and plotted as a function of x_1,x_2. The correlated electron distribution shows the two-electron charge character of the lowest three singlets at low (upper panels, for $W_b=1.5$) and high (bottom panels, for $W_b=5.0$) interdot barriers.

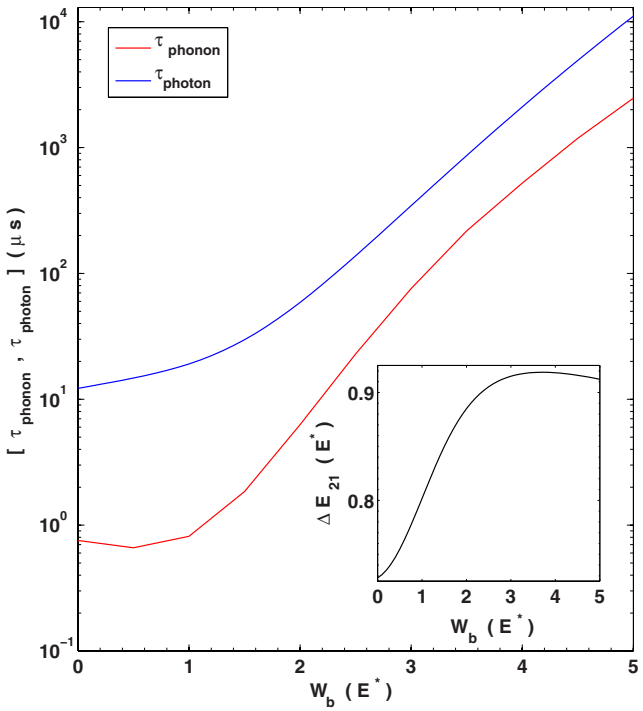

FIG. 4. (Color online) Phonon relaxation time τ_{phonon} (red, lower curve) and spontaneous photon relaxation time τ_{photon} (blue, upper curve) from state $|2\rangle$ to state $|1\rangle$ as a function of the interdot barrier W_b. Inset: energy splitting ΔE_{21} versus W_b.

The phonon emission rate is given by[17–20]

$$\Gamma = \frac{2\pi}{\hbar}\sum_{\mathbf{Q}} \left| \sum_{i=1,2} F_{21}^{(i)}(\mathbf{q}) \right|^2 |G(q_z)|^2 |M(\mathbf{Q})|^2 \delta(W_{21}), \quad (9)$$

where $\mathbf{Q}=(\mathbf{q},q_z)$ and $\mathbf{q}=(q_x,q_y)$. The argument of the delta function is $W_{21}=(|\Delta E_{21}|-\hbar v|\mathbf{Q}|)$, while the coupling term is $M(\mathbf{Q})=|\mathbf{Q}|\hbar g^2/(2v\rho V)$, with $g=8.6$ eV as the GaAs potential constant and $v=4.72\times10^3$ m/s as the longitudinal sound velocity; further, $\rho=5.31\times10^3$ kg/m^3 and V are the crystal electronic density and volume, respectively. The in-plane form factor is

$$F_{21}^{(i)}(\mathbf{q}) = \langle \Psi_2(\mathbf{r}_1,\mathbf{r}_2)|e^{i\mathbf{q}\cdot\mathbf{r}_i}|\Psi_1(\mathbf{r}_1,\mathbf{r}_2)\rangle, \quad (10)$$

while the perpendicular form factor is

$$G(q_z) = \langle \phi(z)|e^{iq_z z}|\phi(z)\rangle. \quad (11)$$

The spontaneous photon emission rate in the host material with refraction index $\eta=\sqrt{\nu}$ is given by[21]

$$\gamma = \eta\frac{\Delta E_{21}^3 |\mu_{21}|^2}{3\pi\epsilon_0\hbar^4 c^3}, \quad (12)$$

where ϵ_0 is the free space permittivity, c is the vacuum light speed, and the dipole moment is

$$\mu_{21} = e\langle \Psi_2(\mathbf{r}_1,\mathbf{r}_2)|\sum_{i=1,2} x_i|\Psi_1(\mathbf{r}_1,\mathbf{r}_2)\rangle. \quad (13)$$

The dipole matrix elements in y and z are zero due to symmetry reasons.

Figure 4 shows that both emission times increase by about 3 orders of magnitude when going from $W_b=0$ to $W_b=5$ so that the respective relaxation rates will completely vanish in the limit of an infinitely high interdot barrier. In the parameter range investigated here, decay can be controlled from the μs to the ms time scales; when the barrier is further increased, population can be frozen over time scales relevant for the macroscopic world. Since the W_b variation in the level splitting ΔE_{21} is small (see inset), the change in decay rates from Eqs. (9) and (12) is mainly due to the decreasing overlap between states $|1\rangle$ and $|2\rangle$, as discussed above. The resonant photon emission wavelength is $2\pi\hbar c/\Delta E_{21} \approx 130$ μm, while the acoustic phonon emission wavelength is $2\pi\hbar v/\Delta E_{21} \approx 2$ nm, the latter being smaller than both lateral and vertical sizes of the DQD. Both wavelengths yield a frequency of ≈ 15 THz.

Note that control of the TMEs in a two-electron DQD comes from controlling the tunnelling between the dots, which is a single-electron property. Therefore, in principle, the TMEs could also be controlled between states with (1,0) and (0,1) charge configurations in a one-electron DQD. However, in practice, it is much more difficult to address and manipulate pure (1,0) and (0,1) configurations since they remain superpositions of bonding and antibonding states at any W_b. In the following, we show that manipulation of a two-electron DQD is, on the other hand, straightforward.

B. Dynamical manipulation of the two-level singlet subspace

Figure 5 demonstrates how the inversion of the two-level system is initially induced, and then how this two-singlet subspace is preserved against decay. The manipulation starts from the ground state $|1\rangle$ of the strongly coupled, highly biased DQD with $\epsilon=-2$ and $W_b=1.5$. First, the population is inverted by changing the bias from $\epsilon=-2$ to $\epsilon=-0.2$ and then back to $\epsilon=-2$ (at $W_b=1.5$), as depicted in panel (a). We use a nonadiabatic technique to invert the system from the ground state $|1\rangle$ to the excited singlet $|2\rangle$. The avoided crossing between $|1\rangle$ and $|2\rangle$ in Fig. 1(a) is ran through fast enough to cause a nonadiabatic population transfer. In order to invert the system, the ramp up and the ramp down have to be chosen in a way that the population transfer during the up-down stages adds coherently, and completely invert the system. After inversion the first-excited state $|2\rangle$ is frozen by ramping up the interdot barrier from $W_b=1.5$ to $W_b=5$ (at $\epsilon=-2$), as shown in panel (b). A one-dimensional (1D) schematic of the DQD potential profile is plotted in the insets for selected positions along the pulse profile. The pulse avoids the symmetric potential, $\epsilon=0$, where state $|2\rangle$ becomes quasidegenerate with state $|3\rangle$.

In panel (c) the time evolution of the population P_i of the four lowest singlets is plotted, as driven by the pulse shape in panels (a) and (b); the time axis in (a) and (b) is the same as in (c). Note that our MCTDHF analysis is converged and

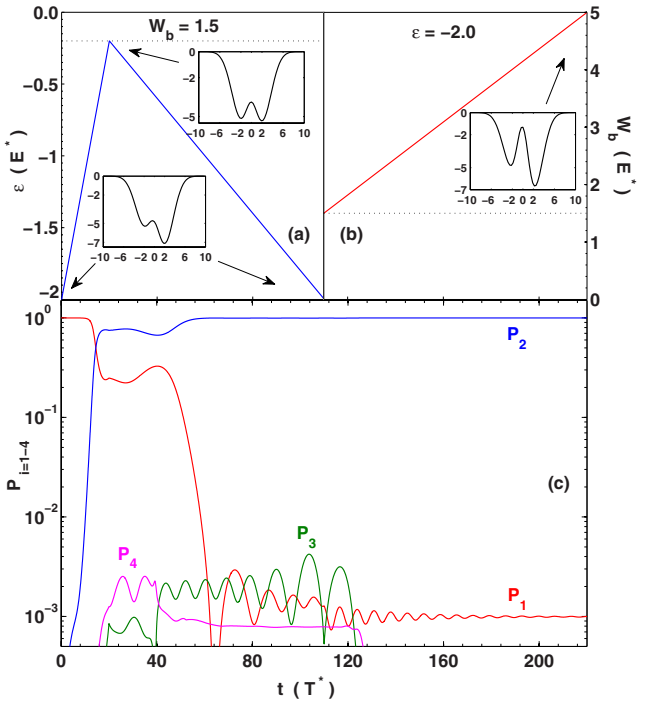

FIG. 5. (Color online) [(a) and (b)] Three-stage pulse profile driving the dynamics: (a) ϵ is increased and decreased back to its initial $\epsilon=-2$ value at $W_b=1.5$ without reaching $\epsilon=0$ and (b) W_b is increased from 1.5 to 5.0 at $\epsilon=-2$. The insets show a 1D view of the DQD potential at the turning points of the pulse, indicated by arrows. (c) Time evolution of the occupation probabilities of the lowest four singlets, $P_{i=1-4}$, as driven by the pulse in [(a) and (b)]. The x axis in (a) and (b) is the same as in (c).

therefore accounts for all singlet states involved in the dynamics. In dependence of the ramp parameters, many more than four states could be populated; for the parameters chosen here on purpose, however, the lowest two singlets are sufficient. The next two excited states are shown in the plot to demonstrate that there is very little leakage (below 10^{-4}) from the lowest two-level Hilbert subspace to higher singlet states.

During ramping of the bias ($0 \leq t \leq 110$), the system crosses the avoided crossing between singlets $|1\rangle$ and $|2\rangle$ twice [check Fig. 1(a)]. This is where most of the population transfer takes place.[7] The ramp parameters were chosen to invert the system; the final population of state $|2\rangle$ reaches $P_2=0.999$ and could be further enhanced via optimum control theory.[22] The population exchange mainly depends on the phase acquired by the system between the two (avoided) crossings.[23] By small changes in the ramp slopes or ramp times, a wave function consisting of arbitrary mixtures of ground and first-excited state can be addressed.

Following our pulse, decay of state $|2\rangle$ is then switched off by ramping up the barrier ($110 \leq t \leq 220$), where the splitting ΔE_{21} follows a smooth behavior [check Fig. 1(b) or inset in Fig. 4]; it changes from ≈ 0.75 to ≈ 0.9 from the low barrier to the high barrier limit. The smallest energy splitting determines the adiabatic time, $t \gg 2\pi/\Delta E_{21} \approx 8.5$, in which the barrier can be ramped up and down with only minor population losses to other eigenstates. Our time interval (110) is chosen so that less than 10^{-4} of state $|2\rangle$ is lost to other states. Indeed, we see in Fig. 5(c) that the population of state $|2\rangle$ remains unchanged as W_b is increased. This shows that freezing of the quantum state is possible without changing its nature by leakage to other bound states. The time for addressing and freezing the system in Fig. 5 is 220 (≈ 12 ps). Over this time, phonon and spontaneous photon decays (μs to ms in Fig. 4) are negligible.

V. DISCUSSION AND CONCLUSION

When the interdot barrier in a two-electron DQD is low, the population of ground and first-excited singlet states can be controlled by time-dependent biasing of the two dots. The population can be insulated against environmentally induced decay by ramping up the interdot barrier, which determines the magnitude of the tunnelling between the dots. In the limit of an infinitely high barrier, single-electron tunnelling is suppressed and the bound states of the two-electron DQD take pure charge configurations. As a result, there remains no overlap between ground and first-excited state so that all one and two-electron TMEs and, therewith, coupling to the environment, vanishes.

We believe that the ability to control TMEs and relaxation is of fundamental importance. An immediate application of this idea to the areas of quantum computation and quantum optics is not trivial and is impeded by obstacles. We would like to discuss some of these difficulties.

First, the two-level singlet subspace investigated here could be used for encoding a two-electron charge[5,24] qubit. Coupling to the environment is a main obstacle in quantum computation.[25] However, freezing the decay allows us only to control the population of such two-level system, but control over dephasing is very limited. Although there is a dephasing component that accompanies decay and that can be eliminated by switching it off, usually the pure dephasing component is dominant.[26] Pure dephasing depends on matrix elements of the type $\langle 1|\hat{O}|1\rangle$ and $\langle 2|\hat{O}|2\rangle$, which do not depend on W_b and cannot be controlled. These matrix elements cause dephasing by randomly changing the energy spacing of the two-level system, ΔE_{21}. An estimation of the pure dephasing time for our system, following Ref. 26, lies in the ns range. This is orders of magnitude faster than the fastest phonon and spontaneous photon decay times in Fig. 4. Therefore, only in combination with control over pure phonon dephasing, our method can be used to create a decoherence-free subspace[27] for quantum computation. Recently, a couple of methods for the control of phonon-induced dephasing were suggested.[28–30]

Second, control over relaxation opens the opportunity to control single-photon emission on demand.[31] However, for the DQD parameters used here, single-photon THz emission is difficult to observe, as relaxation by phonon emission is more efficient by about 1 order of magnitude in Fig. 4, at any interdot barrier. But there exist several ways to enhance photon emission. For example, ΔE_{21} can be increased: (i) by increasing the biasing between the two dots to $\epsilon < -2$ in Fig. 1(a) and (ii) by replacing the first-excited (1,1) state of the two-level subspace with the lowest-lying singlet state with

(2,0) charge character, at $\epsilon=-2$. All the states lying below such highly energetic (2,0) states are of (1,1) or (0,2) character so that TMEs to these states can be controlled by the interdot barrier. This would give an increase in ΔE_{21} by a factor of 2–3; from Eq. (12) one finds that an increase in ΔE_{21} by such amount would already make τ_{phonon} and τ_{photon} comparable. Alternatively, one could also use phonon cavities to suppress phonon emission.[28]

*carlos.destefani@uottawa.ca
†cmcdo059@uottawa.ca

[1] R. Hanson, L. P. Kouwenhoven, J. R. Petta, S. Tarucha, and L. M. K. Vandersypen, Rev. Mod. Phys. **79**, 1217 (2007).
[2] T. Fujisawa, T. Hayashi, and S. Sasaki, Rep. Prog. Phys. **69**, 759 (2006).
[3] J. R. Petta, A. C. Johnson, J. M. Taylor, E. A. Laird, A. Yacoby, M. D. Lukin, C. M. Marcus, M. P. Hanson, and A. C. Gossard, Science **309**, 2180 (2005).
[4] F. H. L. Koppens, J. A. Folk, J. M. Elzerman, R. Hanson, L. H. W. van Beveren, I. T. Vink, H. P. Tranitz, W. Wegscheider, L. P. Kouwenhoven, and L. M. K. Vandersypen, Science **309**, 1346 (2005).
[5] T. Hayashi, T. Fujisawa, H. D. Cheong, Y. H. Jeong, and Y. Hirayama, Phys. Rev. Lett. **91**, 226804 (2003).
[6] M. Pioro-Ladriere, M. Ciorga, J. Lapointe, P. Zawadzki, M. Korkusinski, P. Hawrylak, and A. S. Sachrajda, Phys. Rev. Lett. **91**, 026803 (2003).
[7] C. F. Destefani, C. McDonald, R. M. Abolfath, P. Hawrylak, and T. Brabec, Phys. Rev. B **78**, 165331 (2008).
[8] M. H. Beck, A. Jäckle, G. A. Worth, and H. D. Meyer, Phys. Rep. **324**, 1 (2000).
[9] J. Zanghellini, M. Kitzler, T. Brabec, and A. Scrinzi, J. Phys. B **37**, 763 (2004).
[10] J. Caillat, J. Zanghellini, M. Kitzler, O. Koch, W. Kreuzer, and A. Scrinzi, Phys. Rev. A **71**, 012712 (2005).
[11] R. M. Abolfath, W. Dybalski, and P. Hawrylak, Phys. Rev. B **73**, 075314 (2006).
[12] X. Hu and S. Das Sarma, Phys. Rev. A **66**, 012312 (2002).
[13] D. V. Melnikov and J. P. Leburton, Phys. Rev. B **73**, 155301 (2006).
[14] J. Schliemann, D. Loss, and A. H. MacDonald, Phys. Rev. B **63**, 085311 (2001).
[15] U. Bockelmann and G. Bastard, Phys. Rev. B **42**, 8947 (1990).
[16] C. F. Destefani and S. E. Ulloa, Phys. Rev. B **72**, 115326 (2005).
[17] J. I. Climente, A. Bertoni, G. Goldoni, and E. Molinari, Phys. Rev. B **74**, 035313 (2006).
[18] A. Bertoni, M. Rontani, G. Goldoni, F. Troiani, and E. Molinari, Appl. Phys. Lett. **85**, 4729 (2004).
[19] P. Stano and J. Fabian, Phys. Rev. Lett. **96**, 186602 (2006).
[20] L. Fedichkin and A. Fedorov, Phys. Rev. A **69**, 032311 (2004).
[21] A. Thränhardt, C. Ell, G. Khitrova, and H. M. Gibbs, Phys. Rev. B **65**, 035327 (2002).
[22] U. Hohenester, Phys. Rev. B **74**, 161307(R) (2006).
[23] K. Saito and Y. Kayanuma, Phys. Rev. B **70**, 201304(R) (2004).
[24] J. Gorman, D. G. Hasko, and D. A. Williams, Phys. Rev. Lett. **95**, 090502 (2005).
[25] D. Loss and D. P. DiVincenzo, Phys. Rev. A **57**, 120 (1998).
[26] V. N. Stavrou and X. Hu, Phys. Rev. B **72**, 075362 (2005).
[27] D. Bacon, J. Kempe, D. A. Lidar, and K. B. Whaley, Phys. Rev. Lett. **85**, 1758 (2000).
[28] S. Debald, T. Brandes, and B. Kramer, Phys. Rev. B **66**, 041301(R) (2002).
[29] Y. Takane and T. Murakami, J. Phys. Soc. Jpn. **74**, 2243 (2005).
[30] M. Hentschel, D. C. B. Valente, E. R. Mucciolo, and H. U. Baranger, Phys. Rev. B **76**, 235309 (2007).
[31] B. Lounis and M. Orrit, Rep. Prog. Phys. **68**, 1129 (2005).